Euro. Jnl of Applied Mathematics (2003), *vol.* 14, *pp.* 39–59.
DOI: 10.1017/S0956792502005016 Printed in the United Kingdom

Expulsion of disclinations in nematic liquid crystals

PAOLO BISCARI [1] and TIMOTHY J. SLUCKIN [2]

[1] *Dipartimento di Matematica, Politecnico, Piazza Leonardo da Vinci 32, 20133 Milano, Italy*
Istituto Nazionale di Fisica della Materia, Via Ferrata 1, 27100 Pavia, Italy
email: paolo.biscari@polimi.it
[2] *Faculty of Mathematical Studies, University of Southampton, Southampton SO17 1BJ, UK*
email: t.j.sluckin@maths.soton.ac.uk

(*Received 7 February 2002; revised 27 August 2002*)

We study the interactions between a nematic liquid crystal disclination and the surface of the half-space which bounds it. When strong anchoring conditions are applied on the boundary, the biaxial core of the disclination affects the repulsive force that tends to drive the disclination away from the surface. If we replace the strong boundary conditions with an anchoring potential, the surface-disclination interaction depends on the surface extrapolation length. In particular, the nematic may expel the disclination if the anchoring strength is below a critical value.

1 Introduction

Nematic liquid crystals are so-called because of the dramatic threads which can be seen to run through them when they are viewed through crossed polarizers under a microscope [21]. It is now known that the nematic liquid crystals are anisotropic fluids, characterized at each point by a vector $\mathbf{n} \equiv -\mathbf{n}$, which describes the local preferred molecular direction. The equivalence between $\mathbf{n}$ and $-\mathbf{n}$ reflects the molecular head-and-tail symmetry. Much effort has been expended over the years in developing first a static and then a dynamic theory, based on force balances, which include $\mathbf{n}$ and its spatial derivatives [14, 15, 18, 25, 34]. The threads mentioned above are now known to be line singularities in the director field, along which $\mathbf{n}$ is no longer defined. The singularities are known as disclinations and are the orientational analogues of dislocations in solids. The disclinations in liquid crystals are special in that a half-turn of the director is sufficient to restore it to its original orientation, and a disclination line can be defined by a region around which a closed path including an odd number of half-integral turns can be drawn. We shall return to this in more detail below.

The dilemma in constructing a proper treatment of the full mechanical properties of nematic liquid crystals is not only that the bulk continuum theories developed by Oseen and all subsequent research workers [20, 33, 42] do not formally allow for the separate existence of these disclinations, but that the infinite orientational spatial derivatives which formally occur in their neighbourhood are unphysical and must be removed before a full understanding of the problem can be reached. In view of the fact that disclination lines are

almost ubiquitous in experimental nematic samples, as well as the fact that there has been intense interest in the mechanics of nematic liquid crystals, it is surprising that even now a full mechanical treatment of these systems including defects still eludes us. This paper is a contribution to this debate, and like many other such contributions, is able to proceed because the director description of liquid crystals is embedded in the more general order parameter picture which allows the degree of orientation to be locally varied. The problem we address concerns the location of disclination lines within a confined system, and more specifically the effect of a single boundary on the location of such lines.

A confined nematic liquid crystal is forced to display point or line singularities whenever the boundary conditions imposed on it are topologically nontrivial. Reviews of various aspects of this phenomenon are given in [5, 23, 29]. In particular, the disclinations, which are topologically stable line defects, arise when the director $\mathbf{n}$ rotates an odd multiple of π when we follow its continuous variation around the line. If we denote by k the number of half-turns the director makes around the singular line, this latter is usually named a $\frac{k}{2}$-*disclination*. Half-integer charged disclinations are made possible by the $\mathbf{n} \leftrightarrow -\mathbf{n}$ symmetry that characterizes the nematic. The mere existence of disclinations induces a paradox in the Frank variational theory of nematic liquid crystals [20], since any director field representing a topologically stable disclination apparently possesses an infinite free-energy.

One way to avoid the divergence of the free-energy density close to the disclination is to excise from the system a small volume including the singularity, and then derive the static and dynamic properties of the disclinations by taking the limit as the excised volume goes to zero [9]. Nevertheless, the complete physical description of small regions around the singularities requires an extension of Frank–Oseen–Zocher theory [20, 33, 42], obtained by replacing the director order parameter by the tensor of second-order moments of the local probability distribution of nematic molecules [12, 16]. As a first generalization of the classical theory, it has been shown that the structure and dynamical properties of point [36] and line [24, 37] defects are strongly influenced by the reduction of the degree of orientation, even if one assumes that the nematic remains everywhere uniaxial, and that it becomes isotropic on the defect. Furthermore, numerical and theoretical studies [6, 28, 30, 31, 41] of the core structure have proved that inside the core of a disclination the nematic not only decreases its degree of orientation, but it actually abandons the uniaxial phase, by becoming biaxial in a small, but finite, region surrounding the defect. Recently, tremendous interest in the structure and properties of liquid crystal disclinations has arisen, partly because they can be thought of as laboratory analogues of cosmological structures [8, 11], partly because despite their experimental visibility they are nevertheless extremely complex to describe.

When we consider a nematic disclination confined in a half-space where strong anchoring conditions are applied, the classical limit procedure described above (first applied by Eshelby [17]) yields a repulsive force proportional to the inverse of the distance between the line defect and the surface. On the other hand, in a recent investigation the usual strong anchoring conditions are replaced by an absolutely free boundary, where no anchoring is applied [40]. In this case the disclination is attracted towards the surface, and eventually expelled from the system.

https://doi.org/10.1017/S0956792502005016 Published online by Cambridge University Press

In this paper we study the interaction between a $+\frac{1}{2}$ disclination and a planar surface, when either strong or weak anchoring conditions are imposed at the bounding surface, using the internal Landau–de Gennes potential to analyse the biaxial structure of the core of the disclination. In the former case, we find that if the disclination is sufficiently far away from the surface, the core radius tends to a constant, and the core structure gives no essential contribution to the repulsive force, so that we retrieve the classical results obtained in the limit of a vanishing core. Nevertheless, when the disclination approaches the surface, we find that the core radius shrinks, and the repulsive force increases, doubling its value with respect to the classical prediction.

Furthermore, when a weak anchoring potential is applied to the nematic, we show that the interaction between the surface and the disclination suffers large modifications. If the anchoring is strong enough, the force is still repulsive at all distances, although it remains bounded even when the disclination approaches the surface. If however we decrease the anchoring strength, a critical distance r_{cr} appears, such that the force is repulsive if the surface-disclination distance is greater than r_{cr}, while it becomes attractive below r_{cr}. The results obtained in Richardson [40] (attractive force at all distances) remain valid in the limiting case of vanishing anchoring at the boundary.

The paper is organized as follows. In § 2 we describe the model and the free-energy functional we use. § 3 is devoted to the strong anchoring limit; the surface-disclination force and the core structure will be analysed therein. In § 4 we replace the strong anchoring conditions by a weak anchoring potential and we analyse the qualitative changes suffered by the surface-disclination force. Finally, in § 5 we discuss the results obtained.

2 The model

Let us consider a nematic liquid crystal confined in the half-space $x \geqslant 0$, with a $+\frac{1}{2}$ line defect, parallel to the z-direction and passing through the point $P_\circ = r\,\mathbf{e}_x$. In this section we introduce the free-energy functional and the boundary conditions that we will use to determine a quasi-equilibrium configuration for any given value of the distance r between the disclination and the boundary of the nematic.

2.1 Nematic order tensor

We consider a nematic liquid crystal made up of axisymmetric molecules possessing also head-and-tail symmetry. Even if the molecules tend to arrange themselves in parallel configurations, at any finite temperature a certain degree of disorder will be present throughout the sample. Thus, we describe the local configuration of the nematic liquid crystal by means of the symmetric traceless order tensor $\mathbf{Q}$ of second order moments of the local distribution of molecular orientations, which is defined as follows [12]. Let $f_x(\mathbf{n})$ denote the probability density for a molecule placed at the point $x \in \mathscr{B}$ to have the orientation $\mathbf{n} \in \mathbb{S}^2$. In particular, the head-and-tail symmetry requires $f_x(\mathbf{n}) = f_x(-\mathbf{n})$. The traceless order tensor $\mathbf{Q}(x)$ is defined as

$$\mathbf{Q}(x) := \int_{\mathbb{S}^2} f_x(\mathbf{n}) \left(\mathbf{n} \otimes \mathbf{n} - \frac{1}{3}\,\mathbf{I} \right) \mathrm{d}a.$$

https://doi.org/10.1017/S0956792502005016 Published online by Cambridge University Press

The local physical properties are linked to the degree of symmetry of $\mathbf{Q}$. The nematic is *biaxial* where the three eigenvalues of the order tensor are all different; it is *uniaxial* if two eigenvalues coincide; finally, it locally melts, and becomes *isotropic* if all three eigenvalues coincide and thus $\mathbf{Q} = \mathbf{0}$. We remark that $\mathbf{Q}$ may be either more or less symmetric than the molecules themselves (which are all uniaxial), since it reflects the symmetry of the distribution of the molecules. When the nematic is uniaxial, $\mathbf{Q}$ can be written as

$$\mathbf{Q} = s\Big(\mathbf{n} \otimes \mathbf{n} - \frac{1}{3}\,\mathbf{I}\Big),$$

where $s \in [-\frac{1}{2}, 1]$ is the *degree of orientation* [16] and the unit vector $\mathbf{n}$ is the *director*. In particular s, and thus $\mathbf{Q}$, vanishes if the nematic is isotropic.

We need to describe a $+\frac{1}{2}$ disclination parallel to the z-direction. The symmetry of $\mathscr{B}$ suggests to focus on distributions $\mathbf{Q}$ independent of z with $\mathbf{e}_z$ as one of the eigenvalues

$$\mathbf{Q} = \lambda_1\, \mathbf{e}_1 \otimes \mathbf{e}_1 + \lambda_2\, \mathbf{e}_2 \otimes \mathbf{e}_2 + \lambda_z\, \mathbf{e}_z \otimes \mathbf{e}_z, \tag{2.1}$$

where

$$\begin{cases} \mathbf{e}_1(x,y) = \cos\varphi(x,y)\, \mathbf{e}_x + \sin\varphi(x,y)\, \mathbf{e}_y \\ \mathbf{e}_2(x,y) = -\sin\varphi(x,y)\, \mathbf{e}_x + \cos\varphi(x,y)\, \mathbf{e}_y \end{cases} \quad \text{and} \quad \lambda_z(x,y) = -\lambda_1(x,y) - \lambda_2(x,y), \tag{2.2}$$

so that we will simply refer our configurations to the half-plane $\mathscr{B}_0 := \mathscr{B} \cap \{z = 0\}$.

2.2 Free energy functional

We determine the equilibrium configuration of the nematic liquid crystal by minimizing the bulk free-energy functional

$$\mathscr{F}_{\mathrm{b}}[\mathbf{Q}] := \int_{\mathscr{B}_0} (f_{\mathrm{el}}(\mathbf{Q}, \nabla\mathbf{Q}) + f_{\mathrm{LdG}}(\mathbf{Q}))\, \mathrm{d}a, \tag{2.3}$$

subject to strong boundary conditions or completed with an anchoring energy functional, as we describe below. Using the 1-constant approximation for the elastic part of the free-energy density and the usual expression for the Landau–de Gennes potential [12], the bulk free-energy functional (2.3) can be written as

$$\mathscr{F}_{\mathrm{b}}[\mathbf{Q}] := \int_{\mathscr{B}_0} \left(\frac{\kappa}{2}\, |\nabla\mathbf{Q}|^2 + a\, \mathrm{tr}\,\mathbf{Q}^2 - b\, \mathrm{tr}\,\mathbf{Q}^3 + c\, \mathrm{tr}\,\mathbf{Q}^4 \right) \mathrm{d}a, \tag{2.4}$$

where κ is an elastic constant and, in the nematic phase, $a < 0$, while $b, c > 0$. We remark that a more detailed study of the problem, or the treatment of nematic materials with quite different splay, twist and bend moduli, requires a more specific expression for the elastic potential.[1] Furthermore, numerical simulations [22, 41] prove that the z-symmetry of the equilibrium configurations is broken when the elastic moduli are assumed different.

[1] See Longa *et al.* [26] for the more general rotationally-invariant elastic potential quadratic in the gradient of the order tensor and at most quadratic in $\mathbf{Q}$.

https://doi.org/10.1017/S0956792502005016 Published online by Cambridge University Press

Thus, our symmetrical setting is strictly related to the 1-constant approximation assumed in (2.4).

If $\mathbf{Q}$ is everywhere uniaxial, with constant degree of orientation $s \equiv s_0$, the Landau–de Gennes potential simply contributes an additive constant, and the whole free energy functional (2.4) reduces to the classical 1-constant approximation to Frank's free energy functional [20],

$$\mathscr{F}_{\mathrm{Fr}}[\mathbf{n}] := \kappa\, s_0^2 \int_{\mathscr{B}_0} |\nabla \mathbf{n}|^2 \,\mathrm{d}a = \kappa\, s_0^2 \int_{\mathscr{B}_0} |\nabla \varphi|^2 \,\mathrm{d}a. \tag{2.5}$$

It was first noted by Lyutsyukov [27] that the order-tensor description of nematic liquid crystals avoids the free-energy divergence, since $\mathbb{S}^4$ has no defect in $d = 3$, whereas $\mathbb{P}^2$ does. Thus, on some length scale the $\mathbb{P}^2$ defect would *relax* to the $\mathbb{S}^4$ non-defect. To analyse this relaxation, Lyutsyukov made use of a constraint which has been widely used subsequently [3, 7, 35]. To introduce it, we recall that the parameter b in (2.4) is usually much smaller than both $|a|$ and c. In fact, b is responsible for the isotropic-nematic transition being first order, but it is well-known [12] that this transition is only weakly first order. Thus (see Biscari & Virga [7] for details) we can impose on $\mathbf{Q}$ the constraint

$$\operatorname{tr} \mathbf{Q}^2 = 2\big(\lambda_1^2 + \lambda_1\lambda_2 + \lambda_2^2\big) \equiv -\frac{a}{c} =: \frac{2}{3} s_0^2, \tag{2.6}$$

where $s_0 \in (0, 1]$ represents the degree of orientation preferred in the bulk. The constraint (2.6) automatically minimizes the second- and fourth-order terms in the Landau–de Gennes potential, so that they will be henceforth dropped from the bulk free energy. Recent numerical simulations [1] confirm the validity of the constraint (2.6) in the regime $T \ll T_{\mathrm{NI}}$, while it gives only qualitative understanding of the results close to the nematic-isotropic transition, where a vanishes. To implement (2.6) we introduce a scalar parameter $u(x, y)$ [7], in terms of which we write the eigenvalues of $\mathbf{Q}$ as

$$\lambda_1 = -\frac{s_0}{3}(u - \sqrt{3 - 3u^2}), \quad \lambda_2 = -\frac{s_0}{3}(u + \sqrt{3 - 3u^2}), \quad \lambda_z = \frac{2}{3}\, s_0\, u; \tag{2.7}$$

u may attain all the values in $[-1, 1]$. In particular, when $u = -\frac{1}{2}$ the nematic is uniaxial with degree of orientation s_0 and director $\mathbf{e}_1$, and when $u = -1$ the nematic is uniaxial with degree of orientation $-s_0$ and director $\mathbf{e}_z$; finally, if u takes an intermediate value between -1 and $-\frac{1}{2}$, the nematic is biaxial.

To sum up, we are left with just two parameters to identify the order tensor $\mathbf{Q}$: the angle φ characterizing the eigendirections, and the scalar u, in terms of which all the eigenvalues can be determined.

2.3 Anchoring

We assume that a homeotropic uniaxial anchoring is applied on the nematic at its boundary $\partial\mathscr{B}_0 = \mathscr{B}_0 \cap \{x = 0\}$. Thus, when studying strong anchoring effects, we will enforce the boundary condition

$$\mathbf{Q}(0, y) = \mathbf{Q}_0 := s_0\left(\mathbf{e}_x \otimes \mathbf{e}_x - \frac{1}{3}\mathbf{I}\right) \quad \text{for all } y \in \mathbb{R}, \tag{2.8}$$

https://doi.org/10.1017/S0956792502005016 Published online by Cambridge University Press

which, in terms of φ and u, is equivalent to requiring that

$$\varphi(0, y) = \pi \quad \text{and} \quad u(0, y) = -\frac{1}{2} \quad \text{for all } y \in \mathbb{R}. \tag{2.9}$$

By contrast, the study of weak anchoring effects requires a relaxation of the boundary condition (2.8) by inserting in the free energy functional the anchoring energy

$$\mathscr{F}_{\mathrm{s}}[\mathbf{Q}] := \frac{w}{2} \int_{\partial \mathscr{B}_0} \mathrm{tr}[(\mathbf{Q} - \mathbf{Q}_0)^2] \mathrm{d}\ell. \tag{2.10}$$

Expression (2.10) for the anchoring energy is the most sensible generalization [32] to the order tensor of the classical Rapini–Papoular anchoring energy [39]. Indeed, if we insert in (2.10) both $\mathbf{Q}_0$ as in (2.8) and a uniaxial order tensor $\mathbf{Q} = s_0(\mathbf{n} \otimes \mathbf{n} - \frac{1}{3}\mathbf{I})$, we obtain

$$\mathscr{F}_{\mathrm{RP}}[\mathbf{n}] = w\, s_0^2 \int_{\partial \mathscr{B}_0} (1 - (\mathbf{n} \cdot \mathbf{e}_x)^2) \mathrm{d}\ell.$$

Finally, to enforce a $+\frac{1}{2}$ disclination at the point $P_\circ$, we restrict our attention to angular configurations $\varphi(x, y)$ satisfying the topological property

$$\int_\gamma \left| \frac{d\varphi}{d\ell} \right| \mathrm{d}\ell = \pi \tag{2.11}$$

around any closed curve γ, having natural parameter ℓ and enclosing the point $P_\circ$ in $\mathscr{B}_0$. Condition (2.11) ensures that the planar eigenvectors of $\mathbf{Q}$ complete a half-turn when we follow their continuous variation along γ [5].

2.4 Classical minimizer and beyond

In the classical Frank theory, which we can easily retrieve in our formulation by imposing $u \equiv -\frac{1}{2}$, the Euler–Lagrange equation associated with the functional $\mathscr{F}_{\mathrm{Fr}}$ in (2.5) simply reduces to the Laplace equation in the plane. The minimizing fields φ are thus the harmonic functions which satisfy suitable boundary conditions [9]. In particular, by using an image method, it is possible to construct explicitly an harmonic function φ satisfying both (2.9) and (2.11): let $P_\circ = r\,\mathbf{e}_x$ be a point belonging to the disclination, and let $P_\circ^* = -r\,\mathbf{e}_x$ be its mirror image with respect to the boundary $\partial\mathscr{B}_0$ (see Figure 1). Furthermore, for any point P, we introduce the angle ϑ determined by $(P - P_\circ)$ and $\mathbf{e}_x$, and the angle ϑ^* determined by $(P - P_\circ^*)$ and $\mathbf{e}_x$; then, a harmonic function satisfying both (2.9) and (2.11) is given by

$$\varphi(x, y) = \frac{1}{2}(\pi + \vartheta(x, y) + \vartheta^*(x, y)). \tag{2.12}$$

The well known problem with the classical minimizer (2.12) is that it yields an infinite energy for any value of r. Nevertheless, it is possible to exclude from $\mathscr{B}_0$ a small disc D_ϵ of radius ϵ, centred at $P_\circ$. The energy of the configuration (2.12) and thus the force acting on the disclination can then be computed. Finally one takes the limit $\epsilon \to 0$ of the force.

https://doi.org/10.1017/S0956792502005016 Published online by Cambridge University Press

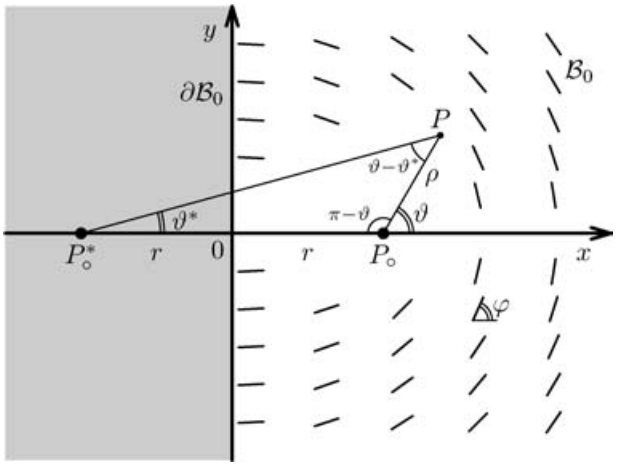

FIGURE 1. Geometry of the $+\frac{1}{2}$ line defect near a planar boundary, parallel to the disclination.

As a result, one finds that [10, 17]

$$\mathbf{F} = \frac{\kappa\pi}{2r}\,\mathbf{e}_x \quad \forall r > 0. \tag{2.13}$$

To go beyond the Frank theory, we still keep the expression (2.12) for φ, but we relax the assumption $u \equiv -\frac{1}{2}$. This permits the degree of orientation of the nematic to decrease, it may even become biaxial. We expect the nematic to leave its most ordered state mainly close to the defect. We therefore parametrize the points in the plane by means of the angle ϑ introduced above, and their distance ρ from $P_\circ$ (or, still better, by means of the dimensionless distance $t := \rho/r$):

$$P = r(1 + t\cos\vartheta)\,\mathbf{e}_x + r\,t\sin\vartheta\,\mathbf{e}_y.$$

The parameter u measures the degree of biaxiality induced in the system by the disclination. Biaxial nematic configurations are strongly penalized both by the Landau–de Gennes potential in (2.3) and by the boundary conditions. Thus, we expect u to be noticeably different from $-\frac{1}{2}$ only close to the singularity and the degree of biaxiality to depend mainly from the distance from the disclination. Consequently, we assume that u depends on t, but not on ϑ.

When we want to impose strong anchoring conditions on $\partial\mathscr{B}_0$, we must require the nematic to be uniaxial there. (The director orientation is automatically orthogonal to the surface as a result of (2.12)). This amounts to requiring $u(t) \equiv -\frac{1}{2}$ for all $t \geqslant 1$, which means that we assume that the minimizing distribution differs from the classical minimizer only inside a circle of radius r, centred at $P_\circ$.

If we substitute (2.2), (2.7) and (2.12) into (2.1), we obtain for the order tensor

$$\begin{aligned}\mathbf{Q} = s_0 u\left(\mathbf{e}_z\otimes\mathbf{e}_z - \frac{1}{3}\mathbf{I}\right) - \frac{s_0}{\sqrt{3}}\sqrt{1-u^2}\,[&\cos(\vartheta+\vartheta^*)\,(\mathbf{e}_x\otimes\mathbf{e}_x - \mathbf{e}_y\otimes\mathbf{e}_y)\\ &+ \sin(\vartheta+\vartheta^*)\,(\mathbf{e}_x\otimes\mathbf{e}_y + \mathbf{e}_y\otimes\mathbf{e}_x)].\end{aligned} \tag{2.14}$$

https://doi.org/10.1017/S0956792502005016 Published online by Cambridge University Press

Then, inserting (2.14) in (2.4), we obtain the following expression for the free-energy:

$$\mathscr{F}_{\mathrm{b}}[u]=\frac{\kappa s_0^2}{3}\int_0^T t\,\mathrm{d}t\int_{\cos\vartheta\geqslant -1/t}\mathrm{d}\vartheta\left[\frac{u'^2}{1-u^2}+\frac{1-u^2}{t^2}\,\frac{1+2t\cos\vartheta+t^2}{1+t\cos\vartheta+\frac{1}{4}t^2}+\frac{r^2}{\xi^2}(1-u\,(4u^2-3))\right], \quad (2.15)$$

where $\xi := \sqrt{\frac{3\kappa}{2bs_0}}$ is the *nematic coherence length*, $T := R/r$, where R is the dimension of the sample (which we will assume to be much greater than any other length that comes into play), $u' := \frac{du}{dt}$, and a constant has been added to the Landau–de Gennes potential in order to raise its minimum value to zero.

3 Strong anchoring

In this section we study the properties of the minimizers of the functional (2.15), subject to the condition $u(t) \equiv -\frac{1}{2}$ for all $t \geqslant 1$. Performing the integral over the angular variable in (2.15), we obtain

$$\begin{aligned}\mathscr{F}_{\mathrm{b}}[u] &= \frac{2\pi}{3}\,\kappa s_0^2\int_0^1\left[\frac{t\,u'^2}{1-u^2}+\frac{1-u^2}{t\left(1-\frac{t^2}{4}\right)}+\frac{r^2}{\xi^2}\,t(1-u\,(4u^2-3))\right]\mathrm{d}t\\ &\quad+\frac{2}{3}\,\kappa s_0^2\int_1^T\left[\frac{3(t^2-2)}{t(t^2-4)}\arctan\left(\frac{t-2}{t+2}\,\sqrt{\frac{t+1}{t-1}}\right)+\frac{3}{2t}\ \arccos\left(-\frac{1}{t}\right)\right]\mathrm{d}t\\ &= \frac{2\pi}{3}\,\kappa s_0^2\int_0^1\left[\frac{t^2\,u'^2}{1-u^2}+\frac{1-u^2}{1-\frac{t^2}{4}}+\frac{r^2t^2}{\xi^2}\,(1-u\,(4u^2-3))\right]\frac{\mathrm{d}t}{t}\\ &\quad+\pi\kappa s_0^2\lg\frac{R}{r}+c_1\,\kappa s_0^2+\mathscr{O}\left(\frac{r}{R}\right),\end{aligned} \quad (3.1)$$

where

$$c_1 := \int_1^\infty\left[\frac{2(t^2-2)}{t(t^2-4)}\arctan\left(\frac{t-2}{t+2}\,\sqrt{\frac{t+1}{t-1}}\right)+\frac{1}{t}\ \arccos\left(-\frac{1}{t}\right)-\frac{\pi}{t}\right]\mathrm{d}t = -1.31474\ldots$$

3.1 Repulsive force on the disclination

The Euler–Lagrange equation associated with the functional (3.1) is

$$\frac{d}{dt}\left(\frac{2\,t\,u'}{1-u^2}\right)=\frac{2\,t\,u'^2\,u}{(1-u^2)^2}-\frac{2u}{t\left(1-\frac{t^2}{4}\right)}+\frac{r^2}{\xi^2}\,t\,(3-12u^2). \quad (3.2)$$

The correct boundary condition to be imposed at $t = 0$ for (3.2) can be deduced from the analysis of the functional (3.1): the integrand is finite in the limit $t \to 0$ only if $\lim_{t\to 0} u^2(t) = 1$ and $\lim_{t\to 0} u'(t) = 0$. Furthermore, and since u is to be continuous at $t = 1$, we have toimpose $u(1) = -\frac{1}{2}$. It can be solved numerically using a relaxation method and yields the minimizing distribution for any value of r. Then, differentiating the resulting minimal free-energy with respect to r, we obtain the quasi-static elastic force acting on the disclination:

$$\mathbf{F} = -\frac{d\mathscr{F}_{\min}}{dr}\,\mathbf{e}_x. \quad (3.3)$$

https://doi.org/10.1017/S0956792502005016 Published online by Cambridge University Press

We note that (3.3) is valid only as long as *backflow* effects can be neglected, that is, only when the translational degrees of freedom do not influence the rotation of the nematic molecules. In fact, the force acting on the disclination is exactly given by (3.3) in the limit of vanishing macroscopic velocities [10], so that we will often refer to the force (3.3) as a *quasi-static* force.

Before embarking upon an analysis of the numerical results, we focus on two asymptotic limits which can be studied analytically.

a) *The large distance limit* $r \gg \xi$. In this limit, the r^2/ξ^2 term dominates in (3.1). Therefore, and to make the coefficient of r^2/ξ^2 as small as possible, the solution of (3.2) remains almost constantly equal to $-\frac{1}{2}$ for all values of $t \gtrsim \xi/r$. Recalling that the first two terms in the functional depending on u are scale-invariant under the transformation $t \mapsto \alpha t$, while the third scales as α^2, we then find

$$\begin{aligned}
&\int_0^1 \left[\frac{t^2 u'^2}{1-u^2} + \frac{1-u^2}{1-\frac{t^2}{4}} + \frac{r^2 t^2}{\xi^2}\,(1-u\,(4u^2-3))\right]\frac{\mathrm{d}t}{t} \\
&\quad\simeq \int_0^{\frac{\xi}{r}} \left[\frac{t^2 u'^2}{1-u^2} + \frac{1-u^2}{1-\frac{t^2}{4}} + \frac{r^2 t^2}{\xi^2}\,(1-u\,(4u^2-3))\right]\frac{\mathrm{d}t}{t} + \int_{\frac{\xi}{r}}^1 \left[\frac{1-\frac{1}{4}}{1-\frac{t^2}{4}}\right]\frac{\mathrm{d}t}{t} \\
&\quad= \int_0^1 \left[\frac{t^2 u'^2}{1-u^2} + \frac{1-u^2}{1-\frac{t^2}{4}} + t^2\,(1-u\,(4u^2-3))\right]\frac{\mathrm{d}t}{t} + \frac{3}{8}\log\frac{4r^2-\xi^2}{3\xi^2}. \qquad (3.4)
\end{aligned}$$

The integral in (3.4) is now independent of r and ξ, and can be interpreted as $\mathscr{F}_{\mathrm{core}}$, the elastic energy stored in the region $t \in [0,1]$ when $r \simeq \xi$. Thus, in this limit,

$$\begin{aligned}
\mathscr{F}_{\min} &= \mathscr{F}_{\mathrm{core}} + \frac{\pi}{4}\,k s_0 \log\frac{4r^2-\xi^2}{3\xi^2} + \pi\kappa s_0^2 \lg\frac{R}{r} + c_1\,\kappa s_0^2 + \mathscr{O}\left(\frac{r}{R}\right) \\
&= \mathscr{F}_{\mathrm{core}} + \frac{\pi}{2}\,\kappa s_0^2 \log\frac{R}{r\xi} + \text{const.} + \mathscr{O}\left(\frac{\xi^2}{r^2}\right) + \mathscr{O}\left(\frac{r}{R}\right). \qquad (3.5)
\end{aligned}$$

Using (3.5) we retrieve the classical result

$$\mathbf{F} = \frac{\pi\kappa s_0^2}{2r}\,\mathbf{e}_x\left(1 + \mathscr{O}\left(\frac{\xi^2}{r^2}\right) + \mathscr{O}\left(\frac{r}{R}\right)\right). \qquad (3.6)$$

Physically, the quantity u is noticeably different from $-\frac{1}{2}$ only in the region $t \in [0, \frac{\xi}{r}]$, or equivalently $\rho \in [0, \xi]$. This implies that the dimension of the core tends to a finite value, closely related to the nematic coherence length, when the disclination is sufficiently far away from the surface. We emphasize that (3.6) is in perfect agreement with the classical result (2.13) if we neglect terms $\mathscr{O}(\xi^2/r^2)$, i.e. if we neglect the core radius.

b) *The small distance limit* $r \ll \xi$. Here, by contrast, the term containing r^2/ξ^2 in (3.1) can be neglected, and u may be far from its bulk value $-\frac{1}{2}$ over the whole interval $t \in [0,1]$ (that is, $\rho \in [0, r]$). Consequently, we have

$$\mathscr{F}_{\min} \simeq \pi\kappa s_0^2 \log\frac{R}{r} + \mathscr{F}_{\mathrm{core}} + \text{const.} + \mathscr{O}\left(\frac{r^2}{\xi^2}\right) + \mathscr{O}\left(\frac{r}{R}\right),$$

https://doi.org/10.1017/S0956792502005016 Published online by Cambridge University Press

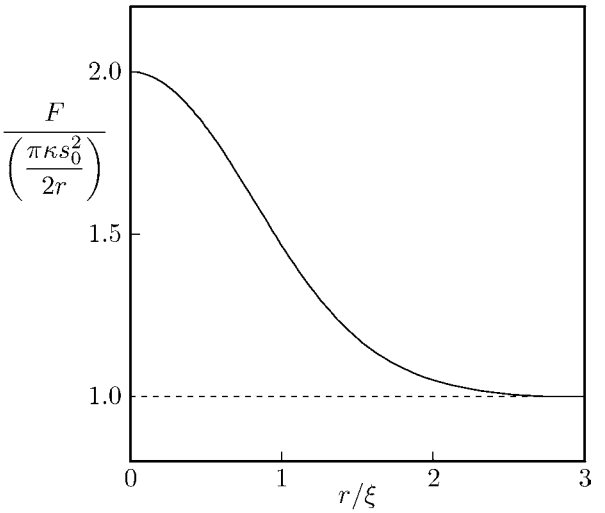

FIGURE 2. Intensity of the quasi-static force acting on a disclination placed at a distance r from a boundary where strong anchoring is applied.

from which we find

$$\mathbf{F} = \frac{\pi\kappa s_0^2}{r}\,\mathbf{e}_x\left(1 + \mathcal{O}\left(\frac{r^2}{\xi^2}\right) + \mathcal{O}\left(\frac{r}{R}\right)\right),$$

so that the coefficient of r^{-1} in the repulsive force *doubles* at short distances.

Figure 2 illustrates the behaviour of the repulsive force acting on the disclination as a function of the distance r from the boundary. The numerical results confirm the analytical limits described above. They give an estimate of the distance from the surface at which the intensity of the repulsive force matches the intensity computed from the classical model. We find that, so long as $r \gtrsim 3\xi$, the classical model can be applied without any serious error.

3.2 Core structure

The degree of orientation of a nematic liquid crystal always decreases close to a defect line. In addition, the present authors [6, 41] and others [27, 28, 35] have shown that the nematic becomes biaxial inside the core of a disclination. The defect itself can be localized to the region where the nematic is uniaxial with a negative degree of orientation. It is always surrounded by a closed surface on which one of the eigenvalues of the order tensor vanishes. Figure 3a, which exhibits the spatial variation of the eigenvalues of **Q** obtained through a numerical solution of (3.2), confirms this prediction.

The concept of degree of orientation is well-defined for uniaxial nematics, and extremely useful in describing non-uniform nematics. It has been generalized [4] to biaxial order tensors:

$$s(\lambda_1, \lambda_2, \lambda_3) := \left(\frac{27}{2}\prod_{i=1}^{3}\lambda_i\right)^{\frac{1}{3}}.$$

https://doi.org/10.1017/S0956792502005016 Published online by Cambridge University Press

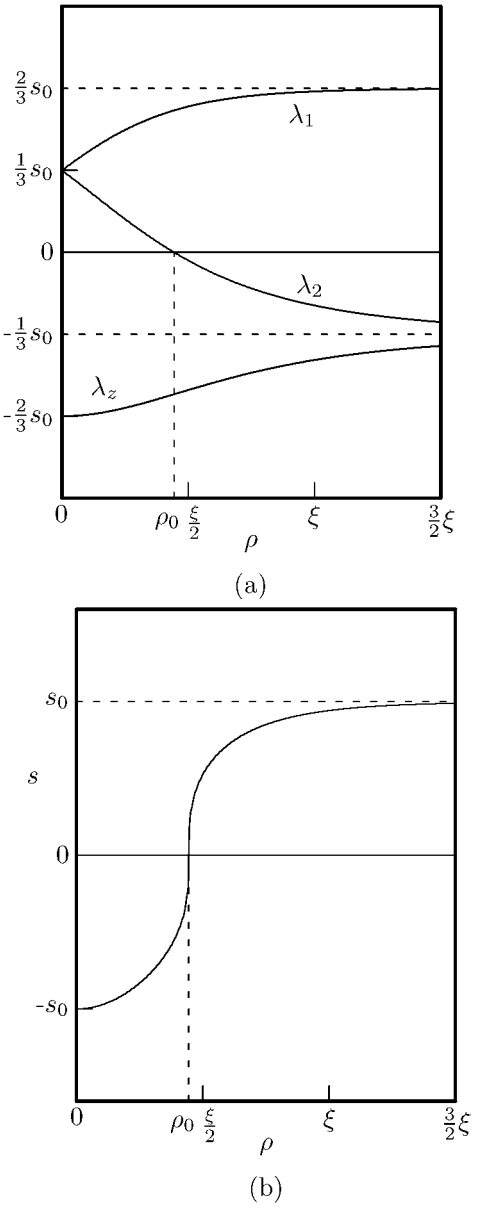

FIGURE 3. Structure of the core of a disclination. (a) Variation of the eigenvalues of the order tensor as a function of the distance from the center of the core. (b) Analysis of the behaviour of the degree of orientation. In both graphs, the disclination is placed at a distance $r = 3\xi$ away from the surface.

Then, s is positive in the bulk but negative inside the defect core. Furthermore, Figure 3b shows that this transition is extremely sharp. It is thus physically as well as mathematically meaningful to define the *core radius* ρ_0 as the distance from the disclination at which one of the eigenvalues, and thus the degree of orientation, vanishes.

https://doi.org/10.1017/S0956792502005016 Published online by Cambridge University Press

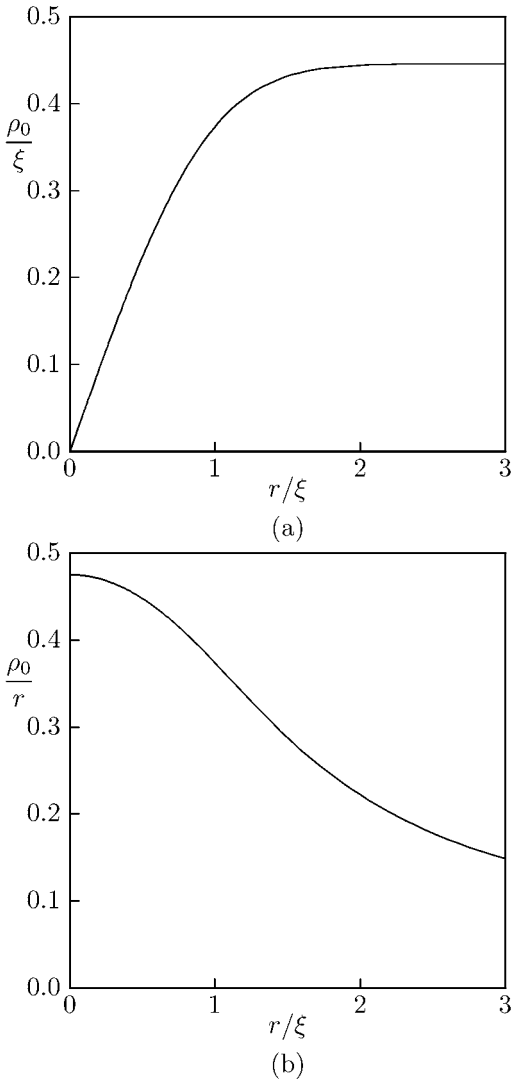

FIGURE 4. Core radius of a disclination line as a function of its distance from the surface. (a) ρ_0 vanishes when the disclination approaches the surface, and tends to its constant bulk value when the defect is very far from the wall. (b) $\rho_0 = \mathcal{O}(r)$ when $r \to 0$.

Figure 4 analyses how the core radius depends upon the distance of the disclination from the surface. In particular, it confirms the asymptotic analysis performed in § 3.1. When the disclination approaches the surface, the core reduces its radius, scaling as r when this latter vanishes (see Figure 4b). By contrast, when the defect moves inside the bulk, the core radius tends to a constant value (see Figure 4a). Furthermore, it is interesting to note that $\lim_{r\to 0} \frac{\rho_0}{r} = 0.475...$ and $\lim_{r\to\infty} \frac{\rho_0}{\xi} = 0.445...$, so that the core radius tends to assume a value which is almost exactly a given fraction (slightly smaller than $\frac{1}{2}$) of the smaller length of the problem, be it r or ξ.

https://doi.org/10.1017/S0956792502005016 Published online by Cambridge University Press

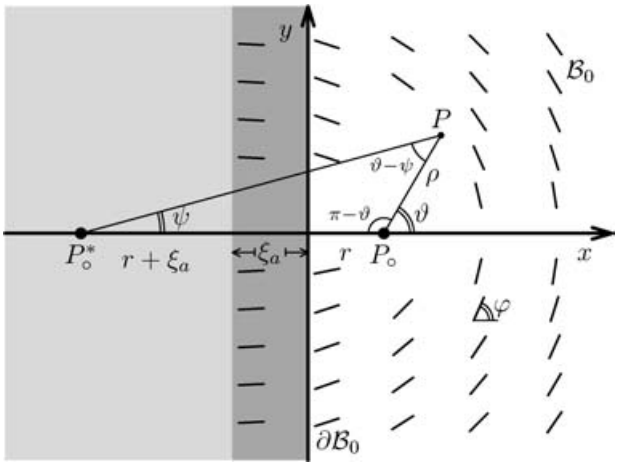

FIGURE 5. Line disclination $P_\circ$ in a nematic liquid crystal close to a weak anchoring surface.

4 Weak anchoring

To study weak anchoring effects, we proceed as follows. First, we add to the free-energy functional the anchoring energy (2.10). Then, we modify the geometrical setting of Figure 1 by introducing the *anchoring length* ξ_a, similar to the cutoff length used in Fournier & Galatola [19]. We make the ansatz (see Figure 5) that the configuration of a nematic subject to weak anchoring coincides with the configuration the same nematic would assume were strong anchoring conditions applied not at its surface $\partial\mathcal{B}_0$, but rather at a distance ξ_a behind the wall. Thus, the trace of the director on the actual surface can be completely different from the preferred, homeotropic, alignment, if ξ_a turns out to be sufficiently large.

The quantity ξ_a is a variational parameter. Increasing values of ξ_a are able to decrease the elastic energy, but at the same time they yield an increase of anchoring energy. Then, for any r and any value of the *surface extrapolation length*, defined as $\zeta := \kappa/w$ [12], we have to determine the optimal configuration by minimizing, with respect to ξ_a, the complete free energy functional $\mathscr{F} := \mathscr{F}_\mathrm{b} + \mathscr{F}_\mathrm{s}$. In general, the two surface lengths ξ_a and ζ do not coincide [38], though they are closely related, as we describe below.

This parametrization also allows for the description of the *expulsion* of the defect from the sample, since r is now no longer necessarily positive. The only requirement to be imposed on the distance is that $r_a := r + \xi_a$ must be positive, so that r may become negative (thus representing an expelled defect) provided that the optimum ξ_a is great enough.

When we insert the order tensors (2.8) and (2.1), with eigenvalues and eigenvectors given by (2.7) and (2.12), in the anchoring energy (2.10), we obtain:

$$\mathscr{F}_\mathrm{s} = \frac{2}{3}\,\kappa s_0^2\,\frac{r_a}{\zeta}\int_{\tilde{r}}^{1}\frac{t}{\sqrt{t^2-\tilde{r}^2}}\left[2+u-\frac{\sqrt{3-3u^2}\,(t^2+2\tilde{r}-2\tilde{r}^2)}{t\sqrt{t^2+4-4\tilde{r}}}\right]\mathrm{d}t$$
$$+\,\kappa s_0^2\,\frac{r_a}{\zeta}\int_{1}^{\frac{R}{r_a}}\frac{t}{\sqrt{t^2-\tilde{r}^2}}\left[1-\frac{t^2+2\tilde{r}-2\tilde{r}^2}{t\sqrt{t^2+4-4\tilde{r}}}\right]\mathrm{d}t, \tag{4.1}$$

https://doi.org/10.1017/S0956792502005016 Published online by Cambridge University Press

where $\tilde{r} := r/r_a$, while the bulk energy (2.4) becomes:

$$\begin{aligned}\mathscr{F}_{\mathrm{b}} = {} & \frac{2\pi}{3}\,\kappa s_0^2 \int_0^{\tilde{r}} \left[\frac{t\,u'^2}{1-u^2} + \frac{1-u^2}{t\left(1-\frac{t^2}{4}\right)} + \frac{r_a^2}{\xi^2}\,t(1-u\,(4u^2-3))\right]\mathrm{d}t \\ & + \frac{2}{3}\,\kappa s_0^2 \int_{\tilde{r}}^1 \left[\frac{t\,u'^2}{1-u^2} + \frac{r_a^2}{\xi^2}\,t(1-u\,(4u^2-3))\right] \arccos\left(-\frac{\tilde{r}}{t}\right)\mathrm{d}t \\ & + \frac{8}{9}\,\kappa s_0^2 \int_{\tilde{r}}^1 (1-u^2)\left[\frac{3(t^2-2)}{t(t^2-4)} \arctan\left(\frac{t-2}{t+2}\sqrt{\frac{t+\tilde{r}}{t-\tilde{r}}}\right) + \frac{3}{2t}\,\arccos\left(-\frac{\tilde{r}}{t}\right)\right]\mathrm{d}t \\ & + \frac{2}{3}\,\kappa s_0^2 \int_1^{\frac{R}{r_a}} \left[\frac{3(t^2-2)}{t(t^2-4)} \arctan\left(\frac{t-2}{t+2}\sqrt{\frac{t+\tilde{r}}{t-\tilde{r}}}\right) + \frac{3}{2t}\,\arccos\left(-\frac{\tilde{r}}{t}\right)\right]\mathrm{d}t. \end{aligned} \tag{4.2}$$

4.1 Asymptotic regimes

Again, we first analyse the functionals (4.1) and (4.2) in the asymptotic regimes representing a disclination very far from or very close to the surface. A complete picture based on numerical computations then follows.

4.1.1 *Large distance limit* $r \gg \xi, \xi_a, \zeta$

The bulk free-energy $\mathscr{F}_{\mathrm{b}}$ can be computed as the free-energy corresponding to a defect placed at a distance r_a from the surface minus the free-energy stored in the strip $x \in [-\xi_a, 0)$, which lies outside the system. In the large distance limit, the whole core region lies inside the bulk, far away from the boundary. Thus, $u \simeq -\frac{1}{2}$ in all the region close to the external surface, and in particular in the strip $x \in [-\xi_a, 0)$. This yields

$$\begin{aligned}\mathscr{F}_{\mathrm{b}} &= \frac{\pi}{2}\kappa s_0^2 \log\frac{R}{r_a\xi} + \text{const.} + \mathscr{O}\left(\frac{\xi^2}{r^2}\right) + \mathscr{O}\left(\frac{r}{R}\right) - 3\kappa s_0^2 \frac{\xi_a}{r}\int_1^\infty \frac{\sqrt{t^2-1}}{t^3}\mathrm{d}t + \mathscr{O}\left(\frac{\xi_a^2}{r^2}\right) \\ &= \mathscr{F}_{\mathrm{str}} - \frac{5\pi}{4}\,\kappa s_0^2 \frac{\xi_a}{r} + \mathscr{O}\left(\frac{\xi_a^2}{r^2}\right) + \mathscr{O}\left(\frac{\xi^2}{r^2}\right) + \mathscr{O}\left(\frac{r}{R}\right),\end{aligned}$$

where $\mathscr{F}_{\mathrm{str}}$ denotes the free energy obtained in the strong anchoring case. Analogously, we obtain for the anchoring energy

$$\mathscr{F}_{\mathrm{s}} = 2\kappa s_0^2 \frac{\xi_a^2}{r\zeta}\int_1^\infty \frac{\sqrt{t^2-1}}{t^3}\mathrm{d}t + \mathscr{O}\left(\frac{\xi_a^3}{r^2\zeta}\right) = \frac{\pi}{2}\,\kappa s_0^2 \frac{\xi_a^2}{r\zeta} + \mathscr{O}\left(\frac{\xi_a^3}{r^2\zeta}\right),$$

and thus

$$\mathscr{F} = \mathscr{F}_{\mathrm{str}} + \frac{\pi}{2}\,\kappa s_0^2\left(-\frac{5}{2}\,\frac{\xi_a}{r} + \frac{\xi_a^2}{r\zeta}\right) + \mathscr{O}\left(\frac{\xi_a^2}{r^2}\right) + \mathscr{O}\left(\frac{\xi^2}{r^2}\right) + \mathscr{O}\left(\frac{r}{R}\right). \tag{4.3}$$

The dominant part in the functional (4.3) is minimized when

$$\xi_a = \frac{5}{4}\,\zeta, \tag{4.4}$$

https://doi.org/10.1017/S0956792502005016 Published online by Cambridge University Press

and its minimum value is

$$\mathscr{F}_{\min} \simeq \mathscr{F}_{\mathrm{str}} - \frac{25\pi}{32}\,\kappa s_0^2 \frac{\zeta}{r}, \tag{4.5}$$

from which we obtain

$$F(r) = -\frac{d\mathscr{F}_{\min}}{dr} = F_{\mathrm{str}} - \frac{25\pi}{32}\,\kappa s_0^2 \frac{\zeta}{r^2} + o(r^{-2}), \tag{4.6}$$

where F_{str} is the value of the quasi-static force when strong anchoring conditions are applied. Equation (4.6) shows that the correction to the quasi-static force tends to decrease its absolute value. Nevertheless, in this limit this correction is $\mathcal{O}(r^{-2})$, and thus negligible if compared to F_{str} itself, which is $\mathcal{O}(r^{-1})$ as (3.6) shows.

4.1.2 *Short distance limit* $r \ll \xi, \xi_a, \zeta$

To analyse this case, we begin by estimating the limiting value approached by the anchoring length ξ_a as $r \to 0$. In this case, the dominant contribution in (4.2) arises from the last integral, so that

$$\mathscr{F}_{\mathrm{b}} = \pi\kappa s_0^2 \log\frac{R}{\xi_a} + \mathcal{O}\left(\frac{\xi_a}{R}\right) + \mathcal{O}\left(\frac{\xi_a^2}{\xi^2}\right),$$

since the last integrand in (4.2) behaves as $3\pi/(2t)$ when $t \gg 1$. For the anchoring energy we obtain:

$$\begin{aligned}\mathscr{F}_{\mathrm{s}} &= w s_0^2\,\xi_a\left[\frac{2}{3}\int_0^1 \left(2 + u - \frac{\sqrt{3-3u^2}\,t}{\sqrt{t^2+4}}\right)\mathrm{d}t + \int_1^{\frac{R}{\xi_a}} \left(1 - \frac{t}{\sqrt{t^2+4}}\right)\mathrm{d}t\right] \\ &= c_2\, w s_0^2\,\xi_a + \mathcal{O}\left(\frac{\xi_a}{R}\right),\end{aligned} \tag{4.7}$$

where $c_2 := \dfrac{2}{3}\displaystyle\int_0^1 \left(2 + u - \frac{\sqrt{3-3u^2}\,t}{\sqrt{t^2+4}}\right)\mathrm{d}t + \sqrt{5} - 1$. Thus,

$$\mathscr{F} = \kappa s_0^2 \left(\pi \log\frac{R}{\xi_a} + c_2\,\frac{\xi_a}{\zeta}\right) + \mathcal{O}\left(\frac{\xi_a}{R}\right) + \mathcal{O}\left(\frac{\xi_a^2}{\xi^2}\right),$$

which is minimized when

$$\xi_a = \frac{\pi}{c_2}\,\zeta,$$

so that we again retrieve that the anchoring length scales with the surface extrapolation length, at least as long as this latter is small enough when compared to the nematic coherence length.

Now, to estimate the quasi-static force on the disclination when it reaches the surface, we must determine the leading terms in r (when $r \to 0$) to (4.1) and (4.2). For the sake of brevity, we skip here the lengthy details of this computation, and we directly give the results:

$$\mathscr{F}_{\mathrm{b}} = \mathscr{F}_{\mathrm{b}}|_{r=0} + \left(c_3 + c_4\,\frac{\xi_a^2}{\xi^2}\right)\kappa s_0^2 \frac{r}{\xi_a} + \mathcal{O}\left(\frac{r^2}{\xi_a^2 + \xi^2}\right),$$

https://doi.org/10.1017/S0956792502005016 Published online by Cambridge University Press

with

$$c_3 := \frac{2}{3}\int_0^1 \left(\frac{tu'^2}{1-u^2} + \frac{4(1-u^2)(1+t^2)}{t(4+t^2)}\right)\frac{\mathrm{d}t}{t} + \frac{1}{2} - 2\pi + \frac{3}{2}\arctan 2,$$

and

$$c_4 := \int_0^1 (1 - u(4u^2 - 3))\,\mathrm{d}t.$$

On the other hand,

$$\mathscr{F}_\mathrm{s} = \mathscr{F}_\mathrm{s}|_{r=0} - c_5 w s_0^2 r + \mathscr{O}\left(\frac{r^2}{\xi_a}\right),$$

with

$$c_5 := \log(2+\sqrt{5}) + \frac{2}{5}\sqrt{5} - c_2 - \frac{8}{3}\sqrt{3}\int_0^1 \sqrt{1-u^2}\,\frac{(t^2+2)\,\mathrm{d}t}{t(t^2+4)^{3/2}}.$$

The quasi-static force on a disclination placed exactly at the surface is thus

$$F(0) = -\left(c_3 + c_4\,\frac{\xi_a^2}{\xi^2}\right)\frac{\kappa s_0^2}{\xi_a} + c_5 w s_0^2 = \frac{\kappa s_0^2}{\zeta}\left[\left(c_5 - \frac{c_2 c_3}{\pi}\right) - \frac{\pi c_4}{c_2}\,\frac{\zeta^2}{\xi^2}\right]. \tag{4.8}$$

The term $(c_5 - c_2 c_3/\pi)$ must clearly be (and turns out to be) positive, since the quasi-static force on the disclination must be repulsive and unbounded in the strong anchoring limit $\zeta \to 0$. Nevertheless, what is really interesting is that both c_4 and c_2 are positive. The former, which measures the internal energy stored in the core, is so because we added a constant to the Landau–de Gennes potential in (2.15) precisely to set the preferred degree of orientation as its zero-level. The latter measures the anchoring energy, apart from a multiplication factor (see (4.7)), and thus it is positive definite by construction (see (2.10)). Thus, the term in the square brackets in (4.8) may change sign when the ratio ζ/ξ becomes sufficiently large, with the result that the boundary force on the disclination may become attractive when the anchoring is sufficiently weak.

4.2 Anchoring length

Figure 6 illustrates how ξ_a depends upon r for different values of the surface extrapolation length. The anchoring length increases when the defect approaches the surface, and it is almost proportional to the surface extrapolation length. This latter effect is enhanced when the ratio ζ/ξ becomes great enough (we recall ζ is typically greater than ξ [2], in some cases even by more than one order of magnitude [13]). Furthermore, Figure 6 confirms the long-distance analytical prediction (4.4), and shows that when ζ becomes of the order of or greater than ξ, (4.4) remains valid at all distances $r \geqslant 0$.

4.3 Expulsion of the defect

Figure 7 shows the fundamental qualitative changes that the weak anchoring induces in the quasi-static force acting on a disclination. In it, positive values of F denote repulsion from the surface, while negative values indicate attraction. As long as $\zeta \lesssim \xi$, the force remains always repulsive, and it monotonically increases when the disclination approaches the surface, even if it tends to a finite limit when $r \to 0$. Furthermore, as we have already

https://doi.org/10.1017/S0956792502005016 Published online by Cambridge University Press

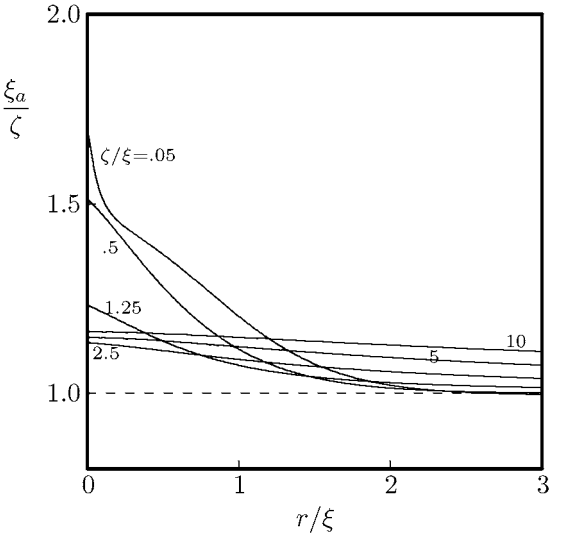

FIGURE 6. Dependence of the anchoring length ξ_a on the distance between the disclination and the surface for the values of the surface extrapolation length indicated therein.

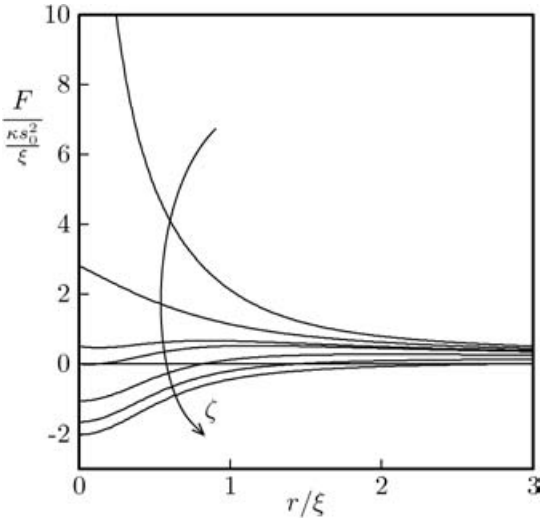

FIGURE 7. Quasi-static force acting on a disclination line placed at a distance r from a weak-anchoring surface. From top to bottom, the graphs refer to the following values of the ratio between the surface extrapolation length ζ and ξ: .05, .5, 1, 1.25, 2.5, 5, and 10.

observed in (4.5), the long-distance behaviour of the quasi-static force does not depend on the anchoring strength.

By contrast, and confirming (4.8), Figure 7 shows that when ζ increases (that is, the anchoring strength decreases) the quasi-static force may first lose its monotonicity, reaching its maximum when the line defect is at a finite distance from the surface. If the anchoring strength decreases further, the surface-disclination force becomes attractive at

https://doi.org/10.1017/S0956792502005016 Published online by Cambridge University Press

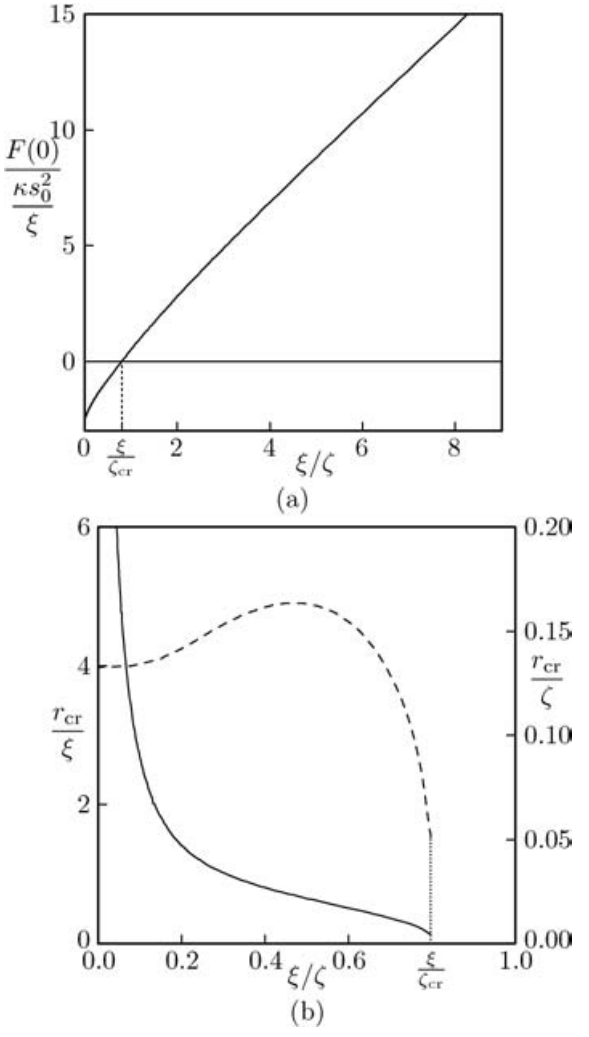

FIGURE 8. (a) Force on a disclination placed exactly at the surface of a nematic liquid crystal as a function of the ratio between the nematic coherence length and ξ and surface extrapolation length ζ. Positive values of $F(0)$ imply that the disclination is pushed towards the nematic bulk, while negative values denote an expulsion of the disclination. (b) Critical value of the distance from the surface at which the quasi-static force on the disclination vanishes, in units of ξ (solid line) and ζ (dashed line). Both graphs are shown as a function of the ratio ξ/ζ.

short-distances, that is, the sample tries to expel the disclination if it comes sufficiently close to the surface.

Figure 8a illustrates in detail the behaviour of $F(0)$ as a function of ζ. The almost linear shape of the curve confirms (4.8). The critical value of the surface extrapolation length at which the surface force changes sign and the expulsion process may arise is given by $\zeta_{cr} = .7974\xi$.

Figure 8b shows the ζ-dependence of the critical distance r_{cr} at which the quasi-static force vanishes. The surface-disclination interaction is attractive when $r < r_{cr}$ and repulsive

https://doi.org/10.1017/S0956792502005016 Published online by Cambridge University Press

at greater distances. It is worth noting that when ζ crosses ζ_{cr}, r_{cr} jumps abruptly from 0 to a value close to 0.13ξ. Furthermore, the dashed line shows that $r_{cr} = \mathcal{O}(\zeta)$ when this latter diverges, so that in the weak anchoring limit we retrieve [40] that the quasi-static force on the disclination becomes attractive at all distances.

We note that r_{cr} is always an unstable equilibrium distance for the disclination. The line defect is driven towards the bulk as long as it remains at a distance $r > r_{cr}$. Nevertheless, if it crosses the critical distance from the surface, it is pushed outwards and eventually expelled from the sample.

5 Concluding remarks

We have studied the quasi-static force that a bounding surface induces on a nematic disclination. More precisely, we have treated in detail the case of a single $+\frac{1}{2}$ defect. However, the methods presented here can also be used to study the boundary interactions of disclinations of greater topological charges or the interactions between two or more defect lines. Our main outcomes are the following:

- When strong anchoring is enforced, the inclusion of a finite biaxial core in the description of the disclination increases the repulsive force that drives the disclination away from the surface. Nevertheless, this strengthening of the repulsive force is a short-range effect, that can be felt only when the distance between the disclination and the surface is of the order of the nematic coherence length.
- The core radius is almost constant (and closely related to the nematic coherence length) as long as the disclination is sufficiently apart from the external surface; otherwise, it scales with the distance from the boundary.
- If we replace the strong anchoring conditions with a weak anchoring energy, a critical distance r_{cr} arises as soon as the the surface extrapolation length ζ becomes greater than the nematic coherence length. The surface-disclination interaction is now attractive for $r < r_{cr}$, but it remains repulsive when $r > r_{cr}$.
- The critical distance r_{cr} is proportional to ζ when this latter diverges. To be more precise, and considering that physically reasonable values for ζ lie in the range $10^{-9} \div 10^{-6}$m., that is $\zeta = 1 \div 10^2 \xi$, we obtain from the dashed line in Figure 8b the estimate $r_{cr} = 0.13\zeta$.

Acknowledgements

This work has been supported by the Brite-EuRam Contract BRRT-CT97-5003 *Liquid crystals: surface properties from basic to applications*. P.B. acknowledges the hospitality of the University of Southampton, where part of this work was carried out.

References

[1] Andrienko, D. (2001) *On the theory and simulation of confined liquid crystals*. PhD Thesis. University of Bristol, UK.

[2] Andrienko, D., Germano, G. & Allen, M. P. (2000) Liquid crystal director fluctuations and surface anchoring by molecular simulation. *Phys. Rev. E* **62**, 6688–6693.

[3] Biscari, P. (1996) Biaxial Persistence Length in Nematic Liquid Crystals. *Mol. Cryst. Liq. Cryst.* **290**, 149–154.
[4] Biscari, P., Capriz, G. & Virga, E. G. (1993) Biaxial Nematic Liquid Crystals. In *Boundary-Value Problems for Partial Differential Equations and Applications: RMA Res. Notes Appl. Math.* **29**, 313–318.
[5] Biscari, P. & Guidone Peroli, G. (197) A hierarchy of defects in biaxial nematics. *Comm. Math. Phys.* **186**, 381–392.
[6] Biscari, P., Guidone Peroli, G. & Sluckin, T. J. (1997) The topological microstructure of defects in nematic liquid crystals. *Mol. Cryst. Liq. Cryst.* **292**, 91–101.
[7] Biscari, P. & Virga, E. G. (1997) A Surface-induced Transition in Polymeric Nematics. *Liq. Cryst.* **22**, 419–425.
[8] Bowick, M. J., Chandar, L., Schiff, E. A. & Srivastava, A. M. (1994) The cosmological Kibble mechanism in the laboratory: string formation in liquid crystals. *Science* **263**, 943–945.
[9] Brezis, H., Coron, J. M. & Lieb, E. (1986) Harmonic maps with defects. *Comm. Math. Phys.* **107**, 649–705.
[10] Cermelli, P. & Fried, E. (2002) The evolution equation for a disclination in a nematic liquid crystal. *Proc. R. Soc. London A* **458**, 1–20.
[11] Chuang, I., Durrer, R., Turok, N. & Yurke, B. (1991) Cosmology in the laboratory: defect dynamics in liquid crystals. *Science* **251**, 1336–1342.
[12] de Gennes, P. G. & Prost, J. (1993) *The Physics of Liquid Crystals.* Clarendon, Oxford.
[13] Dozov, I. & Durand, G. (1998) Surface controlled nematic bistability. *Liq. Cryst. Today* **8**, 1–7.
[14] Ericksen, J. L. (1962) Hydrostatic theory of liquid crystals. *Arch. Rat. Mech. Anal.* **9**, 371–378.
[15] Ericksen, J. L. (1966) Inequalities in liquid crystals theory. *Phys. Fluids* **9**, 1205–1207.
[16] Ericksen, J. L. (1989) Liquid crystals with variable degree of orientation. *Arch. Rat. Mech. Anal.* **113**, 97–120.
[17] Eshelby, J. D. (1980) The force on a disclination in a liquid crystal. *Phil. Mag. A* **42**, 359–367.
[18] Forster, D., Lubensky, T. C., Martin, P. C., Swift, J. & Pershan, P. S. (1971) Hydrodynamics of liquid crystals. *Phys. Rev. Lett.* **26**, 1016–1019.
[19] Fournier, J.-B. & Galatola, P. (2000) Effective anchoring and scaling in nematic liquid crystals. *Euro. Phys. J. E* **2**, 59–65.
[20] Frank, F. C. (1958) On the theory of liquid crystals. *Discuss. Far. Soc.* **25**, 19–28.
[21] Friedel, G. (1922) Les états mésomorphes de la matière. *Ann. Phys. (Paris)* **18**, 273–474.
[22] Hudson, S. D. & Larson, R. G. (1993) Monte Carlo simulation of a disclination core in nematic solutions of rod-like molecules. *Phys. Rev. Lett.* **70**, 2916–2919.
[23] Kléman, M. (1989) Defects in liquid crystals. *Rep. Prog. Phys.* **52**, 555–654.
[24] Kurz, G. (2000) Hydrodynamics of defects in the abelian–Higgs model: an application to nematic liquid crystals. *Ann. Phys.* **282**, 1–30.
[25] Leslie, F. M. (1968) Some constitutive equations for liquid crystals. *Arch. Ration. Mech. Anal.* **28**, 265–283.
[26] Longa, L., Monselesan, D. & Trebin, H.-R. (1987) An extension of the Landau–de Gennes theory for liquid crystals. *Liq. Cryst.* **2**, 769–796.
[27] Lyuksyutov, I. F. (1978) Topological instability of singularities at small distances in nematics. *Sov. Phys. JETP* **48**, 178–179.
[28] Meiboom, S., Sammon, M. & Brinkman, W. F. (1983) Lattice of disclinations: the structure of the blue phases of cholesteric liquid crystals. *Phys. Rev. A* **27**, 438–454.
[29] Mermin, N. D. (1979) The Topological Theory of Defects in Ordered Media. *Rev. Mod. Phys.* **51**, 591–648.
[30] Mottram, N. J. & Hogan, S. J. (1997) Disclination core structure and induced phase change in nematic liquid crystals. *Philos. Trans. Roy. Soc. London A* **355**, 2045–2064.
[31] Mottram, N. J. & Sluckin, T. J. (2000) Disclination cores during the nematic to isotropic phase change. *Liq. Cryst.* **27**, 1301–1304.

[32] Nobili, M. & Durand, G. (1992) Disorientation-induced disordering at a nematic-liquid-crystal-solid interface. *Phys. Rev. A* **46**, R6174–R6177.
[33] Oseen, C. W. (1933) The theory of liquid crystals. *Trans. Far. Soc.* **29**, 883–900.
[34] Parodi, O. (1970) Stress tensor for a nematic liquid crystal. *J. Phys. (Paris)* **31**, 581–584.
[35] Penzenstadler, E. & Trebin, H.-R. (1989) Fine structure of point defects and soliton decay in nematic liquid crystals. *J. Phys. (France)* **50**, 1027–1040.
[36] Pismen, L. M. & Rubinstein, B. Y. (1992) Motion of interacting point defects in nematics. *Phys. Rev. Lett.* **69**, 96–99.
[37] Pismen, L. M. & Rubinstein, J. (1992) Dynamics of disclinations in liquid crystals. *Quart. Appl. Math.* **50**, 535–545.
[38] Priezjev, N. & Pelcovits, R. A. (2000) Surface extrapolation length and director structures in confined nematics. *Phys. Rev. E* **62**, 6734–6738.
[39] Rapini, R. & Papoular, M. (1969) Distorsion d'une lamelle nématique sous champ magnétique. Conditions d'ancrage aux parois. *J. Phys. Colloque C4* **30**, 54–56.
[40] Richardson, G. (2000) Line disclination dynamics in uniaxial nematic liquid crystals. *Quart. J. Mech. Appl. Math.* **53**, 49–71.
[41] Schopohl, N. & Sluckin, T. J. (1987) Defect core structure in nematic liquid crystals. *Phys. Rev. Lett.* **59**, 2582–2584.
[42] Zocher, H. (1933) The effect of a magnetic field on the nematic state. *Trans. Far. Soc.* **29**, 945–57.

https://doi.org/10.1017/S0956792502005016 Published online by Cambridge University Press